

Magneto-electric photocurrent generated by direct inter-band transitions in InGaAs/InAlAs two-dimensional electron gas

Junfeng Dai*,¹ Hai-Zhou Lu*,^{1,2} C. L. Yang,^{1,3} Shun-Qing Shen,^{1,2} Fu-Chun Zhang,^{1,2} and Xiaodong Cui†¹

¹*Department of Physics, The University of Hong Kong, Pokfulam Road, Hong Kong, China*

²*Centre of Theoretical and Computational Physics,*

The University of Hong Kong, Pokfulam Road, Hong Kong, China

³*Department of Physics, Sun Yat-Sen University, Guangzhou, Guangdong, China*

(Dated: November 16, 2018)

We report observation of magneto-electric photocurrent generated via direct inter-band transitions in an InGaAs/InAlAs two-dimensional electron gas excited by a linearly polarized incident light. The electric current is proportional to the in-plane magnetic field which unbalances the velocities of the photoexcited carriers with opposite spins and consequently generates electric current from a spin photocurrent. The observed light polarization dependence of the electric current is explained microscopically by taking into account of the anisotropy of the photoexcited carrier density in wave vector space. The spin photocurrent can be extracted from the measured current and the conversion coefficient of spin photocurrent to electric current is estimated to be $10^{-3} \sim 10^{-2}$ per Tesla.

PACS numbers: 72.25.Dc, 73.63.Hs, 78.67.De

Stimulated by the concept of non-magnetic semiconductor spintronics devices[1], spin injection and detection by optical means have attracted much attention[2–17]. One way to generate spin current is to use linearly polarized optical excitations in bulk III-V semiconductors and quantum wells (QW) with asymmetric band structures induced by the strong spin-orbit coupling (SOC) [11–17]. The left and right circular components of the linearly polarized light generates the same amount of carriers with opposite spins and velocities, leading to a spin photocurrent (SPC) accompanied with a null electric current. The SPC may be generated by various microscopic optical absorption mechanisms[18]. Because spin current carries neither net charge nor magnetization, its measurement becomes a subtle issue[6–9, 12, 13, 19–21]. Experimentally, the detection of the spin current has been realized by converting it to either electric current or magnetization. As a linearly polarized light is injected into a SOC material in the presence of an in-plane magnetic field, the Zeeman splitting induces an imbalance of carriers of opposite spins in \mathbf{k} -space, resulting in electric photocurrent (EPC). The field-induced EPC was systematically studied in the context of the intra-band electron heating, during which abundant spin-dependent excitation and relaxation processes are involved[16, 17].

In this Letter we report the observation of EPC generation via direct interband transition by a linearly polarized light in the presence of an in-plane magnetic field. The EPC is negligible in the absence of the field, and is proportional to the in-plane magnetic field, which indicates the conversion of spin current to electric current by unbalancing the velocities of the photoexcited carriers with opposite spins. The Hall voltage in the presence of a perpendicular magnetic field is used to estimate the magnitude of the SPC when the light is incident on the edge of the sample. The magneto-electric photocur-

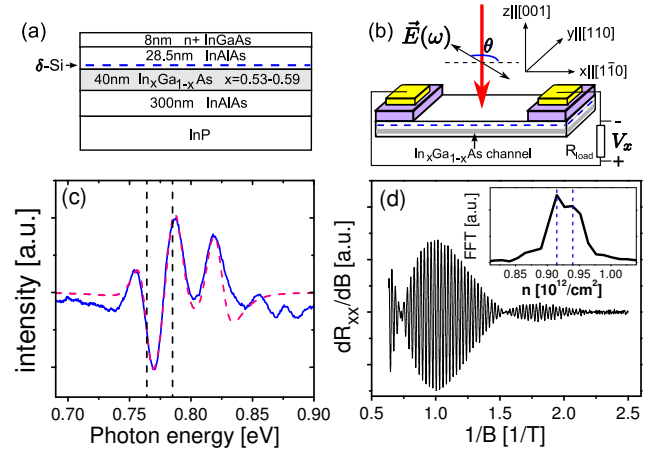


Figure 1: (Color online) (a) [001]-oriented InGaAs/InAlAs quantum well. (b) Illustration of the experiment setup. Linearly polarized light (downward arrow) is normally incident with a polarization angle θ with respect to x -axis. (c) Photo-modulated differential reflectivity spectrum (blue solid curve) at 77 K with the pump light of a DPSS laser at 532 nm. Dashed curve is the spectrum analysis fitting curve[22]. The two lowest interband optical transitions below the photon energy (0.8 eV) are marked by the vertical dashed lines. (d) Shubnikov-de Haas (SdH) oscillation beating pattern of longitudinal magneto-resistance R_{xx} at $T = 2.5$ K. Inset: FFT spectrum of dR_{xx}/dB as a function of carrier concentration n , indicating two spin-split subbands (vertical dashed lines).

rent and the Hall effect allow us to self-consistently evaluate the magnitude of the SPC density from independent approaches. The generation of the SPC and field-induced EPC can be well elucidated by both the symmetry argument[17] and the microscopic model with the anisotropic carrier density in \mathbf{k} -space induced by inter-band optical excitation[11].

The experiment is carried out on the modulation doped

$\text{In}_x\text{Ga}_{1-x}\text{As}/\text{InAlAs}$ QW grown along [001] direction, as shown in Fig. 1(a). The 40 nm InGaAs QW consists of graded indium composition from $x = 0.53$ to 0.59. The mobility and carrier (electron) density were measured as $\mu_m = 12000 \text{ cm}^2\cdot\text{V}^{-1}\text{s}^{-1}$ and $n_e = 2.2 \times 10^{12} \text{ cm}^{-2}$ at room temperatures by Hall measurements. The experiment setup is shown in Fig. 1(b). A $1050 \mu\text{m}$ long (L) and $50 \mu\text{m}$ wide strip of 2DEG channel along [1 $\bar{1}$ 0] and [110] directions was fabricated by standard photolithography and wet etching. Ni/Ge/Au/Ge/Ni/Au metal electrodes was deposited by electron-beam evaporation and then annealed at 450°C for one minute to form Ohmic contact. The linearly polarized light at 1mW normally sheds on the channel through a $10\times$ objective lens and the light spot diameter is approximately $D = 10 \mu\text{m}$. The EPC J_x passing through two terminals is monitored via the voltage drop V_x on a load resistor $R_{\text{load}} = 3.9 \text{ k}\Omega$ with a lock-in amplifier.

The band gap of 0.764 eV is extracted from the photo-modulated differential reflectivity spectrum[22] performed at 77 K as shown in Fig. 1(c). The pump source is a DFB packed laser diode at 1550 nm (0.80 eV) which excites interband transition only in the InGaAs channel. Since the photon energy is well above the band gap and the two lowest interband transition energies [marked by vertical dashed lines in Fig. 1(c)], the dominant optical absorption mechanism here is the direct interband transition, i.e., an electron in a valance band is excited to a conduction band. In the transition, the wave vector of electron \mathbf{k} remains unchanged and its energy is increased by a photon energy $\hbar\omega$. The intra-band transitions within the conduction bands, in which higher-order scatterings by defects and phonons are needed to conserve the momentum, are expected to have much smaller probabilities.

Zinc-blende heterostructures grown along [001] crystallographic direction, like our device, usually have the C_{2v} symmetry[17]. When the measurement is performed along [1 $\bar{1}$ 0] and [110] directions, the dominant SOC is of the Rashba type. The SOC strength α can be examined by the Shubnikov-de Hass (SdH) oscillation of the longitudinal magneto-resistance R_{xx} along the channel[23]. As shown in Fig. 1(d), the SdH beating pattern of the derivative of R_{xx} and the corresponding Fast Fourier transform (FFT) spectrum indicate that there exist two spin-split subbands due to the SOC. The Rashba coefficient is estimated as $\alpha = 4.3 \times 10^{-12} \text{ eVm}$ by $\alpha = \frac{\Delta n \hbar^2}{m^*} \sqrt{\frac{\pi}{2(\bar{n} - \Delta n)}}$, where $\bar{n} = 0.93 \times 10^{12}/\text{cm}^2$ and $\Delta n = 0.025 \times 10^{12}/\text{cm}^2$ are the average value and the difference of the two carrier concentrations extracted from the FFT spectrum[24], and the effective mass $m^* = 0.04m_e$ is assumed.

In the absence of magnetic fields, the two states with opposite wave vectors in each conduction band have opposite spins as required by the time-reversal sym-

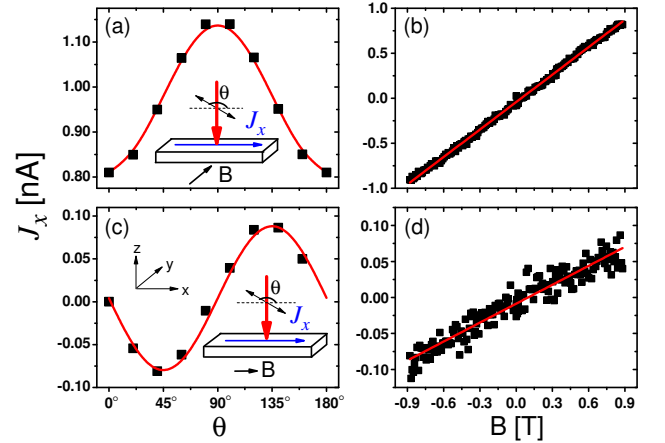


Figure 2: (Color online) Electric photocurrent J_x as a function of the polarization angle θ and in-plane magnetic fields B , along y -axis [(a)-(b)], and along x -axis [(c)-(d)]. $B = 0.9 \text{ T}$ in (a) and (c). $\theta = 20^\circ$ in (b), and $\theta = 120^\circ$ in (d).

metry, resulting in a finite SPC but a null electric current[11, 14, 15, 18]. As expected, we measured a negligible EPC at zero bias without external magnetic field. To explore the SPC, we apply an in-plane magnetic field to lift the spin degeneracy by the Zeeman splitting. The SOC links the spin asymmetry to the imbalance in \mathbf{k} -space and consequently an EPC arises. Fig. 2 shows the EPC J_x induced by the 1550 nm light as a function of in-plane magnetic fields along the y -direction [(a)-(b)] and along the x -direction [(c)-(d)]. The EPCs are linearly proportional to the magnetic field as shown in Figs. 2(b) and 2(d), and shows linear dependence on the light intensity within the maximum laser power of 10 mW. The EPCs demonstrate strong light polarization dependences as shown in Fig. 2 (a) and (c). The relation between the EPC, the magnetic field, and the polarization angle θ can be summarized by

$$J_x(B_x, B_y, \theta) = c_0 B_y + c_y B_y \cos 2\theta + c_x B_x \sin 2\theta, \quad (1)$$

where $c_{0,x,y}$ are constants. According to Fig. 2, c_0 overwhelms $c_{x,y}$, implying unpolarized light (also can be seen as infinite linearly polarized lights) is enough for the observation.

Our observation is consistent with the symmetry argument of C_{2v} group[17]. Because the xz and yz planes coincide with the mirror reflection planes of the C_{2v} group, the polar vectors (such as velocity, current, electric field) along x axis and the axial vectors (such as spin and magnetic field) along y axis transform according to the representation B_1 of the C_{2v} group, while the polar vectors along y and the axial vectors along x directions according to the representation B_2 [25]. As a result, the EPC density in an in-plane magnetic field can be phenomenologically written as[17] $j_\mu = \sum_\nu (\chi^{\mu\nu\nu\bar{\nu}} B_\mu E_\nu E_{\bar{\nu}} + \chi^{\mu\bar{\mu}\nu\nu} B_{\bar{\mu}} E_\nu E_\nu)$, where μ, ν run over $\{x, y\}$, and $\bar{\mu}, \bar{\nu} = y$

if $\mu, \nu = x$, and vice versa. χ is the fourth-rank pseudo tensor that relates the EPC densities to the polarization electric field components $(E_x, E_y) \propto (\cos \theta, \sin \theta)$ of the incident light and magnetic fields (B_x, B_y) . From the above equation, one readily sees the θ -dependence of the EPC.

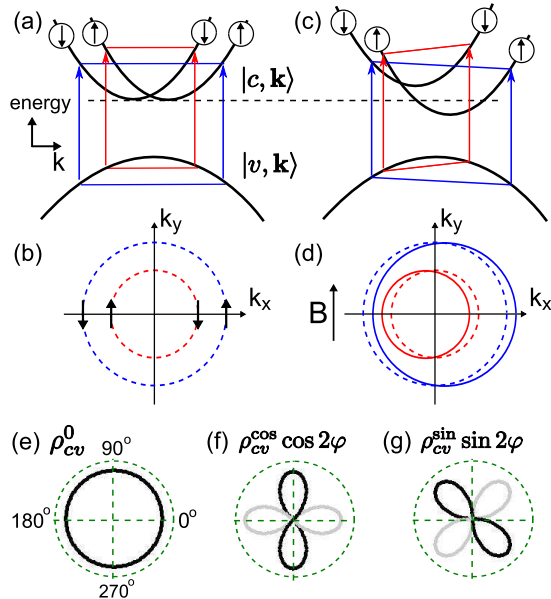


Figure 3: (Color online) [(a) and (c)] Schematic process of direct optical excitations from a valence band $|v, \mathbf{k}\rangle$ to the spin-split conduction bands $|c = \pm, \mathbf{k}\rangle$ at magnetic field $\vec{B}=0$ (a) and \vec{B} along y -axis (c). [(b) and (d)] Constant energy contours (CEC) of photoexcited conduction electrons, which are symmetric (dashed) at $\vec{B} = 0$, and shifted (solid) along k_y (k_x) in the presence of a magnetic field B_x (B_y). The short arrows denote the spin orientations. [(e)-(g)] Wave vector angle (φ)-dependence of photoexcited carrier density $\rho_{cv, \mathbf{k}}$ in Eq. (3) at $\vec{B} = 0$. Only the results on one CEC is shown. Dark (light) curves represent positive (negative) values. $\rho_{cv, 0}^0$ is always positive and overwhelms $\rho_{cv, \cos/\sin}$ terms.

Below we shall present a microscopic picture to further understand the magnetic field and polarization dependences of the EPC in Eq. (1), by considering the anisotropy of the photoexcited carrier density in \mathbf{k} -space[11]. We shall neglect the hole contribution from the valence bands and focus on the conduction electrons, as the lifetime and spin relaxation time of holes in the n-type are much shorter than those of electrons. We shall illustrate our picture by considering two spin-split conduction subbands $|c = \pm, \mathbf{k}\rangle$ described by a Rashba Hamiltonian with C_{2v} symmetry[26], and a valence band $|v, \mathbf{k}\rangle$ [Fig. 3(a)]. In \mathbf{k} -space, the states involved in the interband transition are described by constant energy contours (CEC), which are two perfect concentric circles split by the SOC in the absence of magnetic fields [Fig. 3(b)]. For each state on the CEC, there exists another state with opposite velocity and spin, therefore there is no EPC,

but the difference between two CECs caused by finite effective mass of holes and energy conservation leads to a non-zero SPC. By applying the in-plane field, due to the SOC, the Zeeman splitting of the spin-split conduction bands [Fig. 3(c)] shifts the CECs in \mathbf{k} -space along the direction perpendicular to the B-field [Fig. 3(d)]. This shift then breaks the balance of velocities on the CECs and leads to a finite EPC. The EPC density j_x can be expressed as $j_x = -e \sum_{c, \nu} \int_0^{2\pi} d\varphi \int_0^\infty k dk \delta(k - k_{cv}) \rho_{cv, \mathbf{k}} v_{c\mathbf{k}}^x$, where $\varphi = \arctan k_y/k_x$, $-e$ is the electron charge, k_{cv} are the wave vectors on a CEC and $v_{c\mathbf{k}}^x$ denotes the x -axis velocity of $|c, \mathbf{k}\rangle$. To the linear order in \mathbf{B} ,

$$v_{\pm \mathbf{k}}^x = \left(\frac{\hbar}{m^*} k \pm \frac{\alpha}{\hbar} \right) \cos \varphi \mp \frac{\sin 2\varphi}{2\hbar k} h_x \mp \frac{\cos^2 \varphi}{\hbar k} h_y, \quad (2)$$

where $h_{x(y)}$ is the Zeeman energy along $x(y)$ axis. The \mathbf{k} -dependent photoexcited carrier density $\rho_{cv, \mathbf{k}}$ may be evaluated within the electric dipole approximation, and is found to be well described by the following form in terms of the polarization angle θ at $\mathbf{B} = 0$,

$$\rho_{cv, \mathbf{k}} = \rho_{cv}^0 + \rho_{cv}^{\cos} \cos 2\varphi \cos 2\theta + \rho_{cv}^{\sin} \sin 2\varphi \sin 2\theta. \quad (3)$$

The φ -dependence of $\rho_{cv, \mathbf{k}}$ is explicitly shown in Fig. 3[(e)-(g)]. The above expressions for $\rho_{cv, \mathbf{k}}$ and $v_{\pm \mathbf{k}}^x$ lead to Eq. (1) for J_x [27].

Since the field-induced EPC is well described by the microscopic picture, a direct consequence is that a SPC is expected to exist in the absence of magnetic field. The zero-field expectation value of spin velocity operator along x direction (defined as $\hat{j}_x^{x/y} = \frac{1}{2} \{ \hat{v}_x, \hat{\sigma}_{x/y} \}$, where the superscripts denote the spin orientation, and $\hbar/2$ is dropped for direct comparison with the current), can be found for states $|\pm, \mathbf{k}\rangle$ as $(j_x^x)_{\pm, \mathbf{k}} = \pm \frac{\hbar}{2m^*} k \sin 2\varphi$, $(j_x^y)_{\pm, \mathbf{k}} = (\mp \frac{\hbar}{m^*} k \cos^2 \varphi - \frac{\alpha}{\hbar})$. By comparing $(j_x^{x/y})_{\pm, \mathbf{k}}$ with Eq. (2), we can find that the SPC and the field-induced EPC satisfy a rough but simple relation[28] $j_\mu^y(B=0)/j_\mu(B \neq 0) \approx E_K/h_\mu$, where the Fermi kinetic energy $E_K \approx 10^{-2} \sim 10^{-1}$ eV estimated from the carrier density n_e , and the Zeeman energy h_μ is about 1.2×10^{-4} eV/Tesla (Landé g-factor ≈ 4 [23]). The EPC density $|j_\mu(B \neq 0)|$ is related to the measured J_x in Fig. 2 by $j_\mu(B \neq 0) = en_e \mu_m J_x R_{\text{load}}/L \approx 10^{-5}$ A/m, which assumes the injection is balanced by the drift under the V_x -related built-in field. Summarizing above gives a magnitude of the SPC density $|j_\mu^y(B=0)| \approx 10^{-3} \sim 10^{-2}$ A/m for a 1 mW incident light, and a conversion coefficient from SPC to field-induced EPC about $10^{-3} \sim 10^{-2}$ per Tesla.

To further verify this estimate of the SPC density and conversion coefficient, we employ a Hall measurement in which the light spot acts like a current source in usual Hall bar setup. Besides an in-plane field B_y , we also apply an out-of-plane magnetic field B_z , then scan the light spot across the channel along y axis. From the microscopic picture, it was known that the light spot may

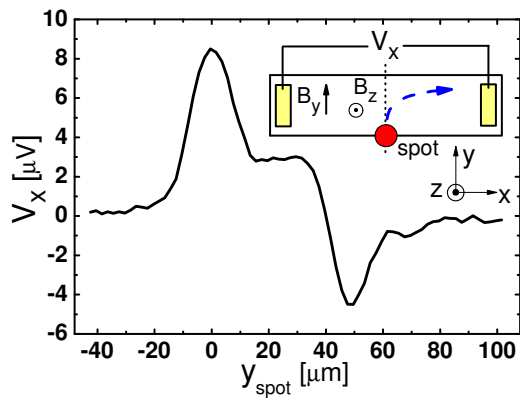


Figure 4: (Color online) Hall voltage V_x as a function of the spot position y_{spot} , in the presence of both in-plane and out-of-plane magnetic fields (B_y and B_z). The inset shows the experimental setup, where a light is shed on the spot at edge of the sample. The scanning path of y_{spot} is marked by the vertical dotted line. The dashed arrow indicates the Hall current trajectory induced by B_z . $B_y = 0.86$ T, $B_z = 0.15$ T, the bar size is $50 \times 1050 \mu\text{m}^2$.

generate photocurrents diffusing out of the spot edge in all directions with the identical current density j_0 . Note that this isotropic j_0 yields no net electric current and is not the field-induced EPC. When the spot is right focused on an edge of the sample [inset of Fig. 4], the anisotropic diffusion leads to a net current Dj_0 normal to the edge and consequently produces a Hall voltage along x direction under the magnetic field B_z . Fig. 4 shows V_x as a function of the spot position y_{spot} (the scanning path is marked by the dotted line). The positive and negative peaks correspond to when the light spot is located at lower and upper edges of the channel, respectively. If the spot is away from the edges, the diffusion of the photocurrent is isotropic and consequently the Hall voltage vanishes. The plateau in Fig. 4 is attributed to the in-plane magnetic field as those in Fig. 2. This photoexcited Hall effect provides another approach to estimate the SPC density. At the edges, Dj_0 is related to V_x by transverse Hall resistivity $\rho_{xy} \approx 2B_z/\pi en_e$, then $j_0 \approx \pi en_e V_x / 2DB_z \approx 2.4 \times 10^{-2}$ A/m at the peaks ($|V_x| \approx 6.5 \mu\text{V}$) in Fig. 4. Approximately, a fraction of $\Delta n/\bar{n} \approx 0.027$ [Fig. 2(d)] of j_0 contributes to the SPC, giving rise to the estimated SPC density $|j_\mu^\nu(B=0)| \approx j_0(\Delta n/\bar{n}) \approx 0.7 \times 10^{-3}$ A/m. Comparing it with the EPC signal (the plateau part) owing to B_y , one could estimate the conversion coefficient of SPC to field-induced EPC at $|j_\mu(B \neq 0)/j_\mu^\nu(B=0)| \simeq 1.7 \times 10^{-2}$ per Tesla. These rough estimates by the Hall effect agree with the low bound by the microscopic model. Furthermore, j_0 can also be evaluated from the conversion of the light power into the photocurrent. If the sample reflectance of 0.3, photon-carrier yield of 30% and the absorption coefficient of $9 \times 10^3 \text{cm}^{-1}$ are assumed,

$|j_\mu^\nu(B=0)| \approx j_0(\Delta n/\bar{n})$ is around 10^{-2} A/m and the conversion coefficient from SPC to field-induced EPC $|j_\mu(B \neq 0)/j_\mu^\nu(B=0)| \simeq 10^{-3}$ per Tesla. These values are well consistent with the high bound obtained by the above microscopic model.

In summary, the measurement of the magnetic-field-induced electric photocurrent supports the signature of the spin photocurrent (SPC) induced via the direct inter-band optical absorption in SOC materials. By two independent approaches with the help of in-plane and out-of-plane magnetic fields, the conversion coefficient of SPC to field-induced EPC is estimated around $10^{-3} \sim 10^{-2}$ per Tesla. The experiment provides a practical way to estimate the magnitude of the SPC density induced by linearly polarized or unpolarized lights.

This work was supported by the Research Grant Council of Hong Kong under Grant Nos. HKU 7013/08P, HKU 7041/07P, and HKU 10/CRF/08.

*These authors contributed equally to this work.

† Email: xdcui@hku.hk

-
- [1] D. Awschalom and M. Flatte, Nat. Phys. **3**, 153 (2007)
 - [2] S. D. Ganichev *et al.*, Nature **417**, 153 (2002).
 - [3] S. D. Ganichev and W. Prettl, J. Phys: Condens. Matt. **15**, R935 (2003).
 - [4] R. D. R. Bhat and J. E. Sipe, Phys. Rev. Lett. **85**, 5432 (2000).
 - [5] J. Hübner *et al.*, Phys. Rev. Lett. **90**, 216601 (2003).
 - [6] M. J. Stevens *et al.*, Phys. Rev. Lett. **90**, 136603 (2003).
 - [7] Y. K. Kato *et al.*, Science **306**, 1910 (2004).
 - [8] J. Wunderlich *et al.*, Phys. Rev. Lett. **94**, 047204 (2005).
 - [9] H. Zhao *et al.*, Phys. Rev. Lett. **96**, 246601 (2006).
 - [10] X. W. He *et al.*, Phys. Rev. Lett. **101**, 147402 (2008).
 - [11] R. D. R. Bhat *et al.*, Phys. Rev. Lett. **94**, 096603 (2005).
 - [12] H. Zhao *et al.*, Phys. Rev. B **72**, 201302(R) (2005).
 - [13] X. D. Cui *et al.*, Appl. Phys. Lett. **90**, 242115 (2007).
 - [14] J. Li *et al.*, Appl. Phys. Lett. **88**, 162105 (2006).
 - [15] B. Zhou and S. Q. Shen, Phys. Rev. B **75**, 045339 (2007).
 - [16] S. D. Ganichev *et al.*, Nature Physics **2**, 609 (2006).
 - [17] V. V. Bel'kov *et al.*, J. Phys.: Condens. Matt. **17**, 3405 (2005).
 - [18] S. A. Tarasenko and E. L. Ivchenko, JETP Lett. **81** 231 (2005).
 - [19] S. O. Valenzuela and M. Tinkham, Nature **442**, 176 (2006).
 - [20] I. Appelbaum *et al.*, Nature **447**, 295 (2007).
 - [21] J. Wang *et al.*, Phys. Rev. Lett. **100**, 086603 (2008).
 - [22] D. E. Aspnes, in: T. S. Moss (Ed.), Handbook on Semiconductors, vol. 2, (North-Holland, New York, 1980), p. 109.
 - [23] J. Nitta *et al.*, Phys. Rev. Lett. **78**, 1335 (1997).
 - [24] G. Engels *et al.*, Phys. Rev. B **55**, R1958 (1997).
 - [25] M. S. Dresselhaus *et al.*, Group Theory Application to the Physics of Condensed Matter (Springer-Verlag, 2008).
 - [26] For simplicity, the microscopic picture in Fig. 3 assumes $C_{\infty v}$ symmetry, which can be generalized to C_{2v} by considering unequal Rashba coefficients along x and y axis.

For $C_{\infty v}$, $|c_x| = |c_y|$ in Eq. (1), which does not hold for C_{2v} .

- [27] Under the same principle of the φ dependence, the linear order terms on \mathbf{B} for $\rho_{cv,\mathbf{k}}$ also lead to almost the same amount of contribution to J_x as those for $v_{c\mathbf{k}}$. For simplicity, this contribution is not explicitly presented.

- [28] The zero-field spin velocity $\propto \hbar k/m^*$ while the magnetic field h_μ induced electron velocity $\propto h_\mu/\hbar k$, so their ratio roughly gives $\frac{\hbar^2 k^2}{2m^*}/h_\mu$, where the extra 2 in front of m^* is due to Ref. [27]. This relation is further interpreted as "kinetic energy over Zeeman energy".